Journal of Energy Storage 70 (2023) 108045

Contents lists available at ScienceDirect

Journal of Energy Storage

journal homepage: www.elsevier.com/locate/est

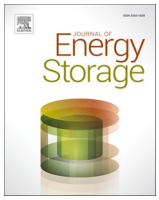

Research Papers

Data-driven prognosis of failure detection and prediction of lithium-ion batteries

Hamed Sadegh Kouhestani [a], Lin Liu [a,*], Ruimin Wang [a], Abhijit Chandra [b]

[a] University of Kansas, Department of Mechanical Engineering, 3136 Learned Hall, 1530 W. 15th St., Lawrence, KS 66045-4709, United States of America
[b] Iowa State University, Department of Mechanical Engineering, 2106 Black Engr, 2529 Union Dr., Ames, IA 50011-2030, United States of America

ARTICLE INFO

Keywords:
Lithium-ion battery
Data-driven
Prognostication
Instability
Deterministic method

ABSTRACT

Battery prognostics and health management predictive models are essential components of safety and reliability protocols in battery management system frameworks. Overall, developing a robust and efficient fault diagnostic battery model that aligns with the current literature is an essential step in ensuring the safety of battery function. For this purpose, a multi-physics, multi-scale deterministic data-driven prognosis (DDP) is proposed that only relies on in situ measurements of data and estimates the failure based on the curvature information extracted from the system. Unlike traditional applications that require explicit expression of conservation principle to represent the system's behavior, the proposed method devices a local conservation functional in the neighborhood of each data point which is represented as the minimization of curvature in the system. Pursuing such a deterministic approach, DDP eliminates the need for offline training regimen by considering only two consecutive time instances to make the prognostication that are sufficient to extract the behavioral pattern of the system. The developed framework is then employed to analyze the health of lithium ion batteries by monitoring the performance and detecting faults within the system's behavior. Based on the outcomes, the DDP exhibits promising results in detection of anomaly and prognostication of batteries' failure.

1. Introduction

Li-ion batteries (LIBs) are becoming ubiquitous in the energy storage units for plug-in or full electric vehicles (EVs). Based on the statistics obtained by Electric Drive Transportation Association (EDTA), EV sales in the United States market have increased from 345 vehicles in 2010 to 601,600 in 2022, with a total of 1.8 million EVs over the twelve-year sales period [1]. This trend has also been observed globally as EV sales reached 2.1 million in 2019 worldwide, boosting the stock to 7.2 million [2]. Although the outbreak of the COVID-19 pandemic dramatically affected the global EV market, prompting the market to plummet over the year 2020 relative to 2019, the projections exhibit an increase in EV stock from 7.2 million to 14 million in 2025 and 25 million in 2030, which accounts for 10 % of global passenger vehicle sales in 2025 and 28 % in 2030 [2,3]. This rapid growth is attributed to the LIBs' superior characteristics over lead-acid, nickel-cadmium, and nickel-metal-hydride batteries, such as lower weight, higher energy density, relatively low self-discharge rate, and longer life cycle [4]. These features and their low emissions impact have played a significant role in the vast adoption of LIBs in various applications, especially in the transportation sector [5].

Although EVs' market is witnessing an unprecedented evolution, the fast adoption of these vehicles requires a more thorough status analysis of the battery performance's functionality and reliability as the primary power source and energy storage unit for EVs. Owing to their rechargeable nature, LIBs operation is subject to different irreversible processes taking place during their charging and discharging cycles and causing capacity fade due to various degradation mechanisms such as decomposition of solid-electrolyte interphase (SEI) on the surface of the electrodes, lithium decrease in electrodes caused by lithium plating or electrolyte oxidation which negatively impacts the cell performance [6–10]. Other deteriorating factors can also cause the LIBs performance, such as electrode decay originating from variations of the volume of active materials during cycles, which will result in induced mechanical stress, a decrease in lithium density of storage sites, and chemical decomposition of electrodes [11]. These cycles severely deteriorate the battery's electrochemical and mechanical constituents, leading to power loss and capacity fade [12,13]. These processes generally result in battery capacity degradation, which usually results in battery failure, with consequences ranging from operational loss to downtime and

* Corresponding author.
E-mail address: linliu@ku.edu (L. Liu).

https://doi.org/10.1016/j.est.2023.108045
Received 12 September 2022; Received in revised form 20 March 2023; Accepted 10 June 2023
Available online 19 June 2023

catastrophic malfunctions [14].

To address the aforementioned issues, over the recent years, numerous studies have been dedicated to proposing proper prediction models for improving the reliability and availability of LIBs [15]. However, current models still suffer from inadequate detailing and inaccurate aging model construction, mostly due to the high complexity and computational burden associated with nonlinear models [16].

Furthermore, in some cases, the effect of current and state of charge on the proposed models may be overlooked, resulting from data insufficiency to develop a detailed model and the complexity of the computational models [17]. On the other hand, failure of LIBs does not necessarily occur due to a single battery degradation mechanism. Instead, it may stem from detrimental coupling effects during the battery's operational lifetime [18]. Due to accuracy and computational complexity challenges, most existing remaining useful life (RUL) and health prediction models focus on singular degradation effect and usually ignore the integrated deterioration mechanisms that are normally involved in the aging model of batteries associated with the inadequacy of current health estimation tools.

The above challenges necessitate a robust and reliable predictive framework for prognostics and health monitoring (PHM) under a complexly hostile working environment. PHM is a multifaceted discipline for evaluating the extent of deviation or degradation of the system and is intended to detect incipient components or system faults [19]. Traditionally, PHM techniques use either model-based (or physics-based) approaches, data-driven approaches, or hybrid methods which combine model-based methods with data-driven models [20–22]. In model-based or physics-based approaches, mathematical equations, such as differential equations, are employed to represent the system's performance. Also, the constitutive parameters or coefficients in the differential operators must be known a priori. Then, statistical estimation tools relying on parity relations are used to discover, isolate, and potentially predict fault within the system's behavior [21,23]. Numerical predictive models based on conservation principles are then used to make such prognostications. A variety of model-based (or physics-based) methods have been proposed over recent years to predict the system state and failure of LIBs. Aggab et al. proposed a unifying model-based prognosis integrated with time series prediction method to estimate the end of life of LIBs [24]. Li et al. developed an electrochemical model-based power prediction approach to study the safety and operation of LIBs [25]. Xiong et al. devised a recognition degradation approach to predict the remaining capacity of LIBs and illustrated the effectiveness of the model to estimate the failure [26]. Chen et al. proposed a model-based fault diagnosis algorithm to study the external short circuit and failure of LIBs [27].

On the contrary, data-driven approaches use statistical pattern recognition tools and historical information to detect anomalies in parameter data, isolate faults, and estimate a product's end of life [28,29]. Generally, data-driven methods do not rely on the product-specific knowledge of the material parameters and failure mechanisms; in contrast, the product's constitutive parameters are evaluated by in situ monitoring based on the provided data and the anomaly in the system is detected without needing to know the failure modes [29]. However, they largely rely on availability of training data that are used to observe abnormal patterns and predict an accurate representation of the model. Lately, numerous data-driven approaches have been proposed, such as Artificial Neural Networks (ANN) [30], Support Vector Machine (SVM) [31], Gaussian Process Regression (GPR) [32], particle filter (PF), and fuzzy logic [28]. For instance, Cadini et al. presented a data-driven particle filter diagnosis method to predict the end of life of LIBs [33]. Dong et al. proposed a Brownian data-driven model integrated with extended Kalman filter to predict the end of life of batteries [34]. Nuhic et al. used a SVM method to estimate the state of health and remaining life of LIBs. Ji et al. developed a deep learning model to model the aging and health of LIBs. Wu et al. used an online method based on feed-forward neural network (FFNN) and Importance Sampling (IS) to estimate the LIBs end of life [30]. Zhao et al. proposed a new approach combining fault diagnosis results with statistical methods to construct a reliable battery model [35].

Despite the recent advances in developing data-driven methods, such techniques still face major challenges. The primary bottleneck in using data-driven methods is their direct dependency on pre-existing data that are used to train the models which are not always available. Moreover, current data-driven algorithms easily neglect the importance of properly tuning hyperparameters, regularization and selection of proper loss functions that are important for achieving high accuracy models. When too many hyperparameters are adjusted simultaneously, rendering conclusive solutions becomes hard to achieve [36]. Considering the above challenges in the current state of the art of LIBs prognostics and health management, it is crucial to introduce new methods that can eliminate the current drawbacks in the battery predictive models with high prognostication accuracy. To achieve this goal, the models need to minimize their dependency on the presence of explicit expression for conservation principles that are widely used in model-based or physics-based approaches on one hand and reduce the reliance to large amount of training data in data-driven models on the other hand. Thus, exploring novel venues to develop such models becomes imperative.

In this context, this study aims at proposing and developing a novel data-driven approach called data-driven prognosis (DDP) that estimates the relevant constitutive parameters of the system in situ and detects deviations from the degradation dynamics or behavioral pattern of the system. The proposed DDP approach circumvents the need for offline training and relies solely on in situ measurements. This is achieved by pursuing a deterministic approach rather than a probabilistic approach and considering only two consecutive time instances at each step of the simulation to make the prognostication that are sufficient to extract the behavioral pattern of the system. Although the DDP uses a deterministic framework, the solution's stochastic nature arises naturally from the underlying assumption regarding the order of the potential function and the number of dimensions considered. It can be easily modified to be employed for any system in which such a priori testing is difficult or even impossible to conduct due to circumventing the need for offline training. DDP functions under the principle that at each two consecutive time instances, a conservation functional is locally assigned at each observation point which is assumed to be piecewise quadratic in this work, whereas the global format is unknown. The conservation principle is then used to minimize the system's local curvature at each step of the time which is defined as the fault criteria in this study. Using such an approach, a dimensionless length scale containing a correct combination of geometric and materialistic information of the system is extracted and estimated. Ultimately, the system stability is represented as its ability to minimize the local curvature below a critical value which is defined as the inverse of length scale at each observation point. Therefore, the stability characteristics of the system are dependent upon the dimensionless length scale in addition to the local curvature information. Such an approach eliminates the need for explicit conservation and constitutive functionals. The instability forecasting capability of the DDP method has been verified to be accurate previously in a balloon burst experiment [37]. After developing the framework the DDP was employed to analyze the health status of LIBs by detecting faults within the system's performance and predict the global instability of the batteries. This is done by using a set of data extracted from experimental program in which two LIBs were tested and relevant information were obtained and fed into the algorithm. The remainder of the paper is organized as follows: the DDP model development, including the algorithms, introduced in Section 2. Section 3 briefly details the experimental program, followed by results in Section 4 and the conclusion in Section 5.

2. Model development

In the proposed approach, it is assumed that a conservation principle

Table 1
Path dependency index (PDI) categories.

Category	Definition of the category
1	Complete stability: (abs(k[a])/abs(k-long)) <1 and (abs(k)/abs(k-short)) <1
2	Long-term stability & short term instability: (abs(k)/abs(k-short)) > 1
3	Long-term instability & short term stability: (abs(k)/abs(k-long)) > 1
4	Provisional stability: Changing mode mixity might cause local instability
5	Short-term and long-term instability: local instability cannot be controlled by altering mode mixity
6	Short-term and long-term instability in dimension > 1
7	Short-term and long-term instability in dimensions > 2
8	Chain length > short-term critical chain length, PDI > 5
9	Chain length > long-term critical chain length, PDI > 5

[a] k = kappa (curvature).

is applied to the observation points, which may be the conservation of energy, conservation of linear and angular momentums, or all of the above. In the proposed DDP method, it is assumed that the total momentum in the system is conserved. Following such a logic, a dimensionless form of length scale value containing the correct combination of geometric and material parameters, is derived from the conservation functional. The length scale values are then used to capture the magnitude of curvature in the system as a form of absorption or release. To do so, suppose we have an observable body or phenomena with a finite number of observation points. At each of these observation points, information is collected at discrete instants of time in multiple dimensions. These points are collectively considered, and a normalized relationship is constructed for each pair of points for the entire set of observation points. Calling the two observation points A and B, at a specific dimension d, the normalized relationship, a_d^{AB}, is defined as Eq. (1):

$$a_d^{AB} = \frac{u_d^A - u_d^B}{u_d^A + u_d^B + 2\overline{m}_d} \tag{1}$$

where u_d^A and u_d^B are the measured values at dimension d at points A and B. The parameter $\overline{m}_d$ is a small constant, to be determined later. The purpose of such a normalized relationship is to have an understanding of the behavior of points in a pairwise manner. Next, a governing conservation principle is applied at each point that must be satisfied at all times, considering that the system remains in a conservative state. The principle of conservation of linear momentum is chosen for this purpose. Furthermore, it will be attempted to satisfy the three canonical requirements: equilibrium, compatibility, and constitutive laws. To develop such a model, as the first attempt, a piecewise second-order utility function is assumed to sufficiently describe the system's interactions. However, the nature of the piecewise quadratic potential function can differ from one point to the other. Additionally, it is assumed that the objectivity in the system is also ensured at all times,

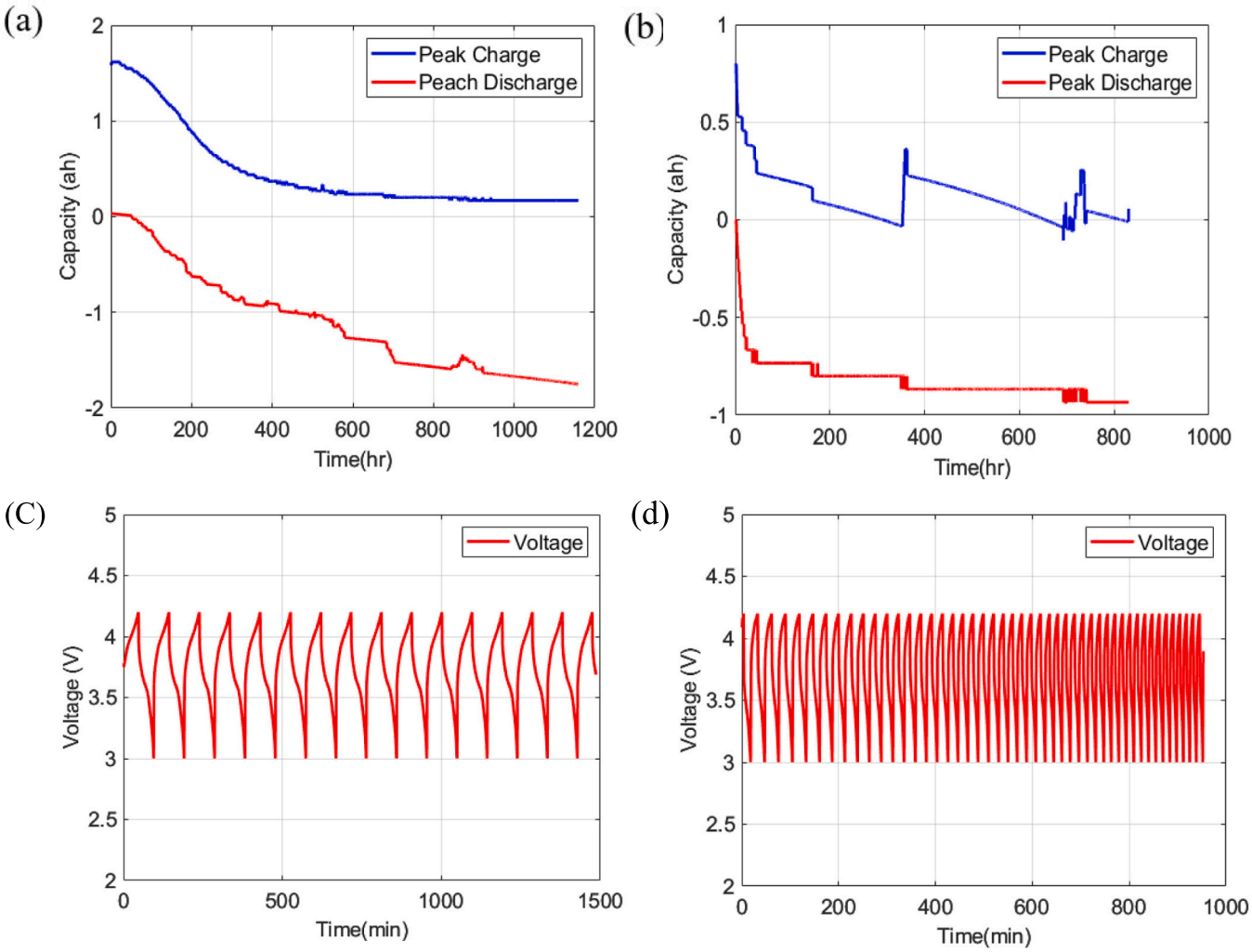

Fig. 1. Experimental result of the battery peak charge discharge capacity and voltage: a) 48D battery capacity @ 1C, b) 54D battery capacity at @ 2C, c) 48D battery voltage, d) 54D battery voltage.

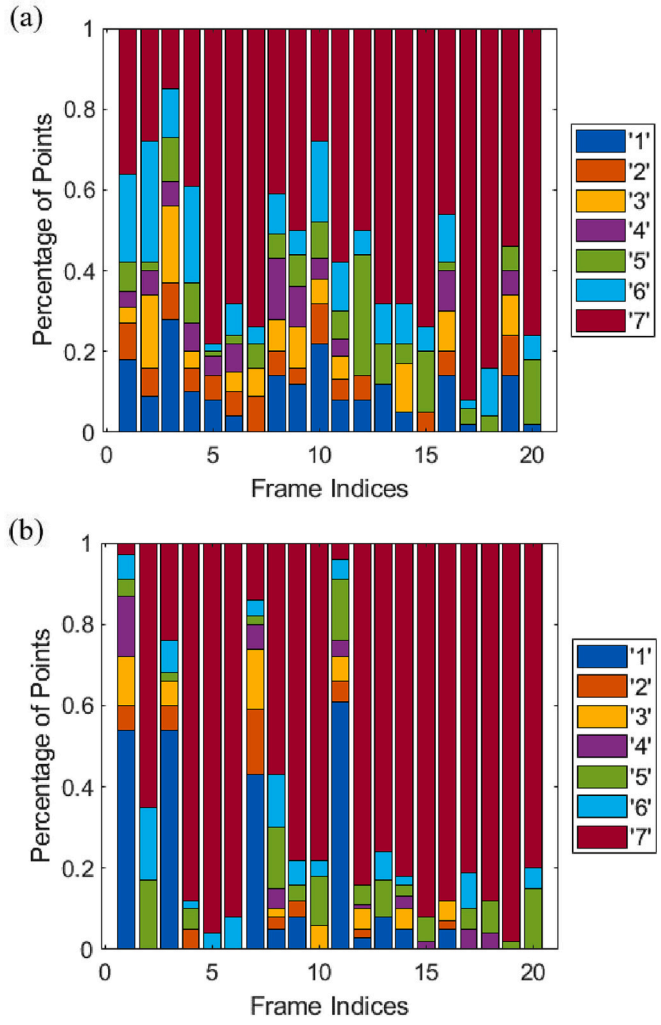

Fig. 2. Path dependency index for peak charge capacity: a) 48D battery @ 1C, b) 54D battery @ 2C.

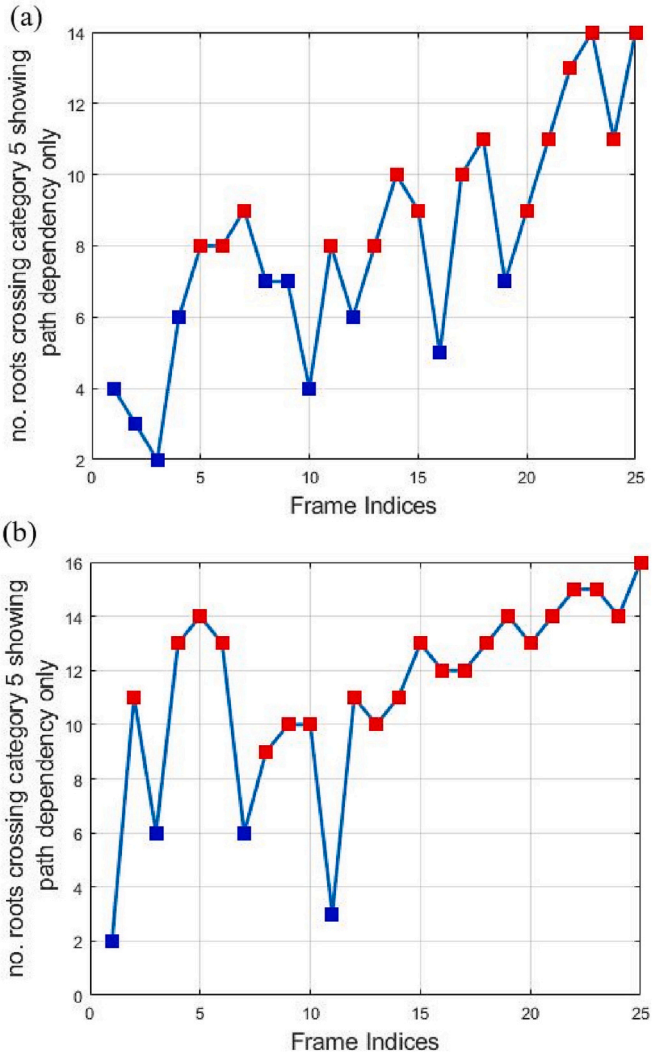

Fig. 3. Number of roots having category >5 showing path dependencies only in peak charge: a) 48D battery @ 1C, b) 54D battery @ 2C.

implying that the state of the observed system remains unchanged due to rigid body transformations of the reference frame. Doing so ensures the satisfaction of three canonical requirements. Enforcing these requirements, the system is described by considering the conservation of linear momentum in the neighborhood of point A as [37,38]:

$$R_i^A - \beta_{ik}^A \times \Delta H_k^A = 0 \tag{2}$$

where R_i represents the rank (long-term rank) in dimension i at point A. H_k represents the Borda count (short-term rank) at dimension k at point A. ΔH_k represents the change in the Borda count in dimension k during a time step. Borda count in this context, is calculated by constructing a global skew-symmetric matrix that represents the normalized value for each pair of points and summing them at each row or column. Long-term rank is similarly computed by performing one round of iteration using Eq. (3).

$$a_{ij}^1 = a_{ij}^0 + CF \bullet \sum_{k \neq i,j} \left(a_{ik}^0 + a_{kj}^0 \right), \forall i, j \tag{3}$$

where a_{ij}^0 denotes the given initial pairwise differences between i,j, a_{ij}^1 represents the revised pairwise differences after one iteration defined late on, and ***CF*** is a positive constant described as the confidence factor.

For more details about these parameters, readers are encouraged to refer to [39–42]. The parameter β_{ik} is a non-dimensional quantity that represents a second-order norm of the length scale around a point, which is described as:

$$\beta_{ik} = \left(\frac{1}{\Delta t^2} \right) \times \left(\frac{\rho}{E_{ijkl}} \right) \times \left\| L_i L_j \right\| \tag{1}$$

Here, Δt is the change in time step, ρ is the density and E_{ijkl} is the tangent modulus. Substituting the above expressions into Eq. (2), we obtain the general format for the length scale that is expressed as:

$$E_{ijkl} \left[\frac{R_i}{L_l L_j} \right] = \frac{\rho}{(\Delta t)^2} \times \Delta H_k \tag{2}$$

The length scale is defined as the region of validity along a particular dimension in which the linearization of the governing equation is valid. Furthermore, the conservation of angular momentum and the symmetry of the potential function about an interchange of the state variables are enforced. This is administered by requiring interchangeability of (i and j), (k and l) as well as (i,j and k,l) as pairs. Existence of symmetrical potential function, is also mandated by the work conjugacy requirement of stress and strain [43]. After enforcing all the symmetry requirements, a general expression of the potential function at each observation point is expressed as:

$$\frac{E_{ijkl}}{2} \times \left[\frac{R_i}{L_l L_j} + \frac{R_j}{L_k L_i} + \frac{R_k}{L_j L_l} + \frac{R_l}{L_i L_k} \right] = \frac{\rho}{(\Delta t)^2} \times \left[\Delta H_i + \Delta H_j + \Delta H_k + \Delta H_l \right] \tag{3}$$

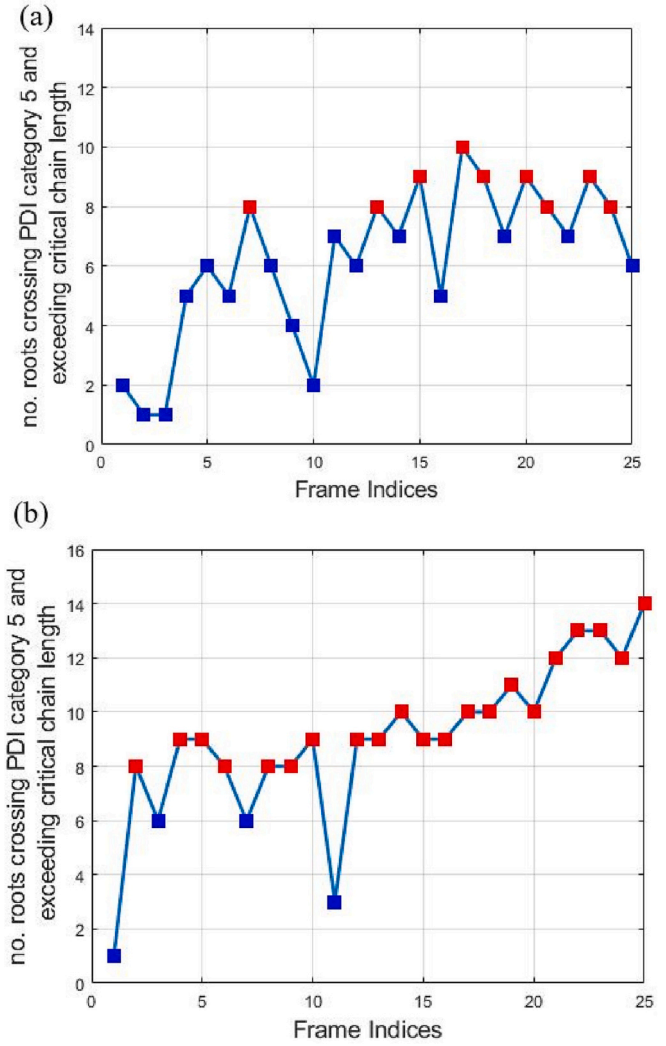

Fig. 4. Number of roots having category >5 and having chain length greater than number of points in peak charge capacity: a) 48D battery @ 1C, b) 54D battery @ 2C.

The number of solutions for the potential function is dependent upon the number of dimensions involved in the system. In general, the number of solution, also called the number of roots, is 2^{dimsize} (dimension size). At each point, there are a number of dimensions; the root at each point in each dimension corresponds to the roots at every other dimension. Thus at each point at each dimension, the number of equations is equal to the number of dimensions. For instance, if there are 4 dimensions at a specific point, the number of equations is 4. The roots then can be obtained by solving the set of (d x d) simultaneous equations at each observation point. Thus, the proposed strategy requires solving N matrices (when N is number of observation points) each with dimension d, resulting in a very computationally efficient and massively parallelizable scheme.

The component $\overline{m}_d$ essentially sets the datum, and the coordinate of the origin is set at $-\overline{m}_d$ in the corresponding dimension. Owing to the fact that only a least square approximation is used for calculating $\overline{m}_d$, it is applied universally to all points (with the purpose of setting a same datum for all observation points). However, the values of $\overline{m}_d$ in different dimensions are different and are set independently.

Next, the obtained values of volumetric and shear length scales are used to compute the shear and volumetric curvatures. This is achieved by defining a composite curvature as (Eq. (7)):

$$\kappa = \alpha\kappa_v + (1-\alpha)\kappa_s \tag{4}$$

where, κ_v and κ_s are volumetric and shear curvatures, respectively, that are calculated as:

$$\kappa_v = \frac{(R \times \overline{L}_v - H \times \widetilde{\overline{L}}_v)}{\left(\left(\overline{L}_v^2\right) \times \widetilde{\overline{L}}_v\right) \times \left(1 + (H/\overline{L}_v)^2\right)^{1.5}} \tag{5}$$

$$\kappa_s = \frac{(R \times \overline{L}_s - H \times \widetilde{\overline{L}}_s)}{\left(\left(\overline{L}_s^2\right) \times \widetilde{\overline{L}}_s\right) \times \left(1 + (H/\overline{L}_s)^2\right)^{1.5}} \tag{6}$$

$\widetilde{\overline{L}}$ represents the homogenized version of $\overline{L}$, α is the proportion by which volumetric curvature takes place and R and H are rank and Borda count that were described previously. Substituting the volumetric and shear curvature values in Eq. (7), it is attempted to minimize the composite curvature by setting the LHS of the equation to zero and obtain the α values at each point across each dimension. Then, the mean of all squared α values are taken and used in Eq. (6) again using that unique value to obtain the composite curvature.

To identify a specific range for the alpha values, we employ the composite stress equation that is described by [43]:

$$\sigma_{ij} = \lambda\varepsilon'\delta_{ij} + 2G\left(\varepsilon_{ij} - \frac{1}{3}\varepsilon'\sigma_{ij}\right) \tag{7}$$

where λ and G are bulk and shear modulus, respectively, and are defined as:

$$\lambda = \frac{\nu E}{(1+\nu)(1-2\nu)} \tag{8}$$

$$G = \frac{E}{2(1+\nu)} \tag{9}$$

By comparing Eq. (10) with Eq. (7), a similarity is noticeable between these two equations and their volumetric and shear components. The range of proportionality is obtained from this resemblance and considering the proportions of:

$$\frac{\lambda}{2G} = \frac{\alpha}{1-\alpha} = \frac{\nu}{(1-2\nu)} \tag{10}$$

We already are aware of the range of Poisson's ratio that is in the range of $-1 < \nu < 0.5$. hence, the range of α should be between $-0.5 < \alpha < 1$. By computing alpha, the mode mixity between the dilatational and shear modes in the problem is assigned.

2.1. Post processing [37,38]

The proposed method relies on a set of criteria that evaluates the magnitude of instability in the system. These criteria use the information that was obtained from length scale and curvature calculations. They are discussed in the following sections.

2.1.1. Categorizing the instability of observation points

The next step in model development is the assignment of the path dependency index (PDI) to the observation points following the determination of curvature and associated length scales which is a type of data classification. The PDIs are divided into nine possible categories each representing a magnitude of instability, in which category 1 represents no instability and category 9 denotes complete instability (Table 1). All 16 roots (in 4D) for the length scale obtained from the previous step have to be examined individually for this stage. The severity of instability will be measured based on the ratio of the absolute value of the obtained composite curvature equation divided by the absolute value of curvature that is determined from the reciprocal of length

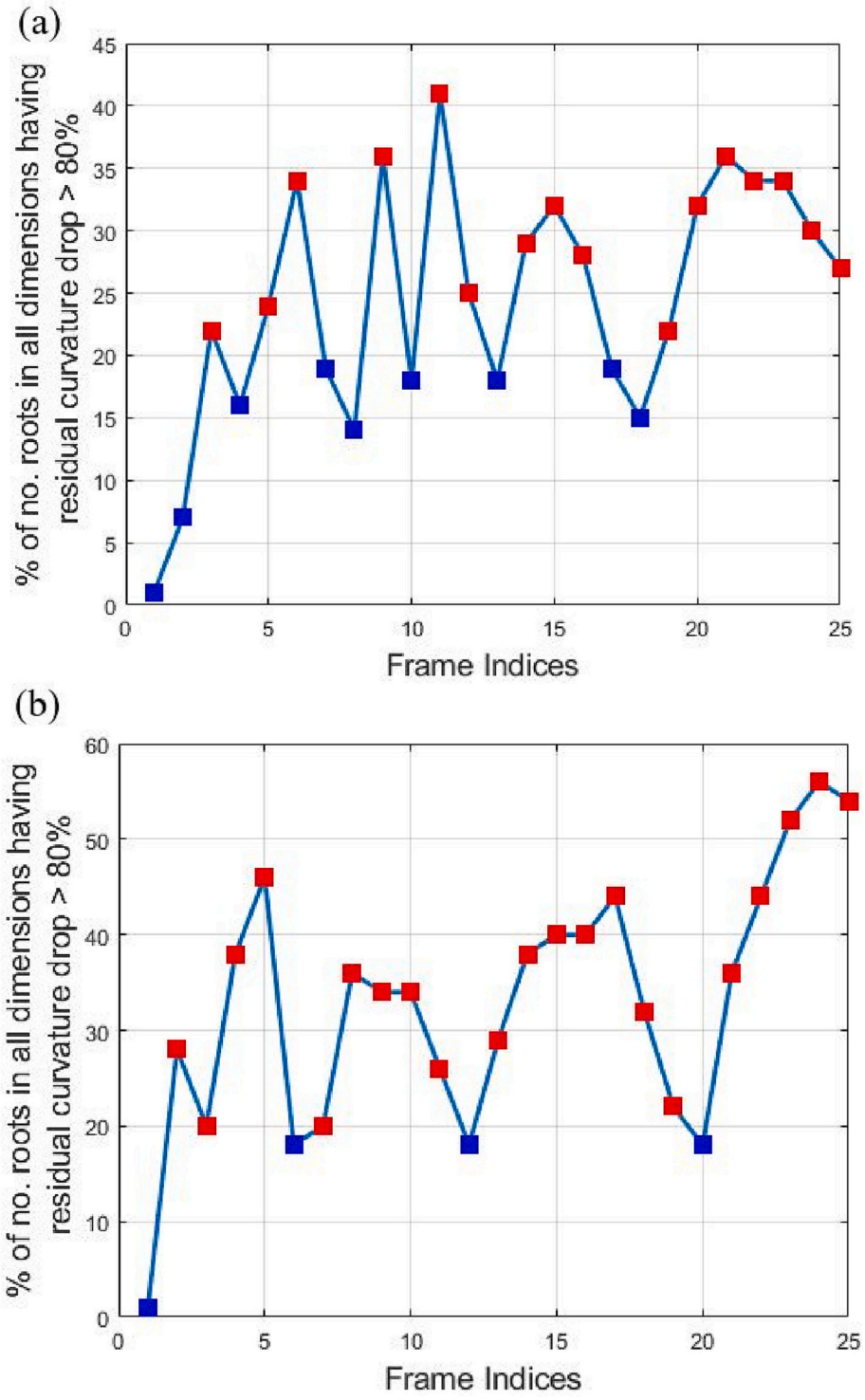

Fig. 5. Number of roots having residual curvature drops >80 % in peak charge capacity: a) 48D battery @ 1C, b) 54D battery @ 2C.

scales, i.e. $\overline{L}$ and $\widetilde{\overline{L}}$; we call them kappa short and kappa long, respectively. If the obtained value is less than one in both cases, we conjecture that the observation point does not exhibit short or long-term instability. Depending on whether the point reaches short-term or long-term instability, it will be categorized based on Table 1. The initial 7 categories are related to PDI, and the remaining 2 categories, i.e. categories 8 and 9, are designed for further post-processing, which depicts the global transcendation index or GTI. Suppose the observation point falls in the category 5 or more. In that case, we conclude that the point enters the path dependency stage and might illustrate local instability with the potential to enter the global instability phase.

2.1.2. *Determination of chain length*

Following the assignment of PDIs, it is necessary to check how long a defect or a chain of possible unstable points might continue in either direction in the order of their ranks, called chain length. This calculation is done to facilitate the determination of chain length in abstract systems such as genetics or economic systems that is associated with the constitution of energy exchange pathways. For a point to enter an energy

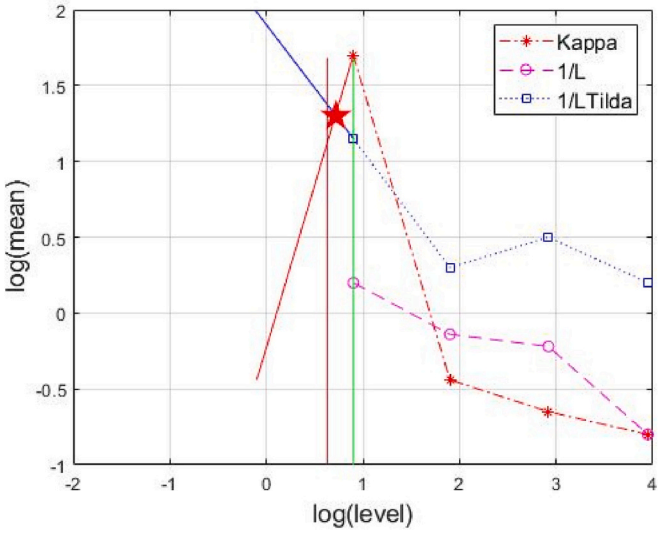

Fig. 6. Zoom out plot – Chain length calculation in peak charge capacity (48D battery).

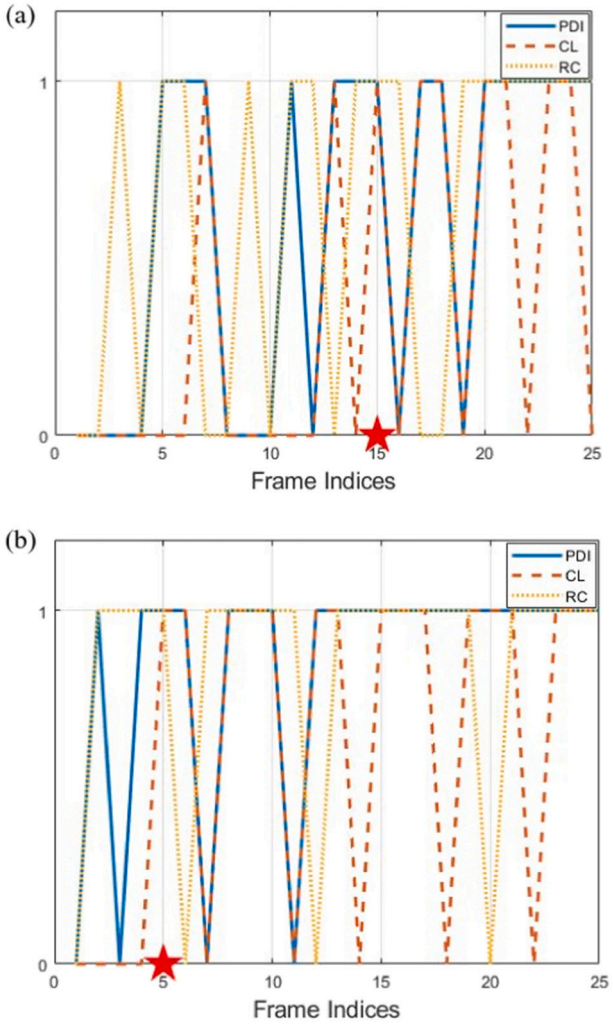

Fig. 7. Composite failure prediction for: a) 48D battery @ 1C, b) 54D battery @ 2C.

exchange pathway, it must exhibit a PDI ≥ 5. This threshold is identified as the critical gateway to transcendation to the next aggregated scale in the hierarchy and might enter to global transcendation phase.

2.1.3. Global transcendation index

After the system enters the path dependency phase, if it meets two additional measurements, it is conjectured that it is progressing toward failure. These measurements are: (1) the locally path-dependent observation points form a chain, whose length exceeds a critical threshold value, (2) the aggregated level of the system exceeds a critical threshold called residual curvature. Upon meeting these measurements, the system enters the global transcendation stage and the category 8 is assigned to the point if it reaches PDI > 5, and GTI > 0 in one dimension, and category 9 is assigned if both of these conditions are satisfied in multiple dimensions.

2.1.4. Aggregation or zoom-out procedure

The aggregation procedure (or zoom-out plot) is followed and calculated to determine the critical chain length and residual curvature (also called aggregated curvature) of the system for each instant of time. The residual curvature provides a measure of the potential energy exchange rate of the system with its surrounding environment. According to the definition of zoom out procedure, the observed curvature for a conservative system should be approximately zero in instances when the stand-off distance of the observer is both zero and infinity. Such a procedure serves as a mean to identify the critical length of the energy exchange pathway that is required for the local instabilities to transcend to global scales. The energy exchange rate also needs to exceed a critical threshold value to meet the sufficiency conditions for transcendence of local instabilities to global scale. Because the critical energy release rate is related to the system's constitutive property, which is determined normally by conducting offline testing, the proposed method assumes that almost all of the energy stored along the exchange pathways gets released when the local instability transition to a global scale. Hence, the energy rate fluctuates rapidly and falls nearly to zero during such a transcendent procedure. This rapid fluctuation in the energy exchange rate is used in this method to account for a trigger initiated every time the energy rate drops >80 % during a step (which is arbitrarily chosen and associated with the inherent noise and computational burdens). Therefore, a point reaches the global transcendent stage following exceeding a critical chain length and 80 % or more drop in the energy release rate during a single time step, constituting a GTI >0.

The failure prediction relies on three primary measurements, and for a system to initiate instability and it needs to meet the following metrics: (1) the system enters the path dependency phase, (2) long-term chain formation is triggered, and (3) residual curvature (or energy release rate) is dropped by 80 % or more. A system is said to approach to failure if it meets these conditions simultaneously and the prognosis scheme makes a prediction based on the instant of time that these measurements were met. It should be noted that the method was previously validated based on the studies conducted in [37,38].

3. Experiments

The experiments were mainly aged battery cycling tests. Since the proposed DDP requires large amount of data (i.e., charge capacity, discharge capacity, current, and voltage) at each data collection and sampling to analyze, we selected commercially available rechargeable lithium batteries that are naturally aged in our lab and quickly failed during testing. Cost and equipment limiting factors led to the decision to use Kokam superior lithium polymer pouch-sized batteries that are 95 mm in height and 3.5 mm in depth, and 64 mm wide. As suggested by the manufacturer, the maximum charge current and voltage were set to below 2020 mA and 4.2 V; the maximum discharge current and voltage were 3030 mA with a cut-off voltage of 3.0 V. The battery-rated capacity, nominal voltage, and cycle life are 2100 mAh, 3.7 V, and 500

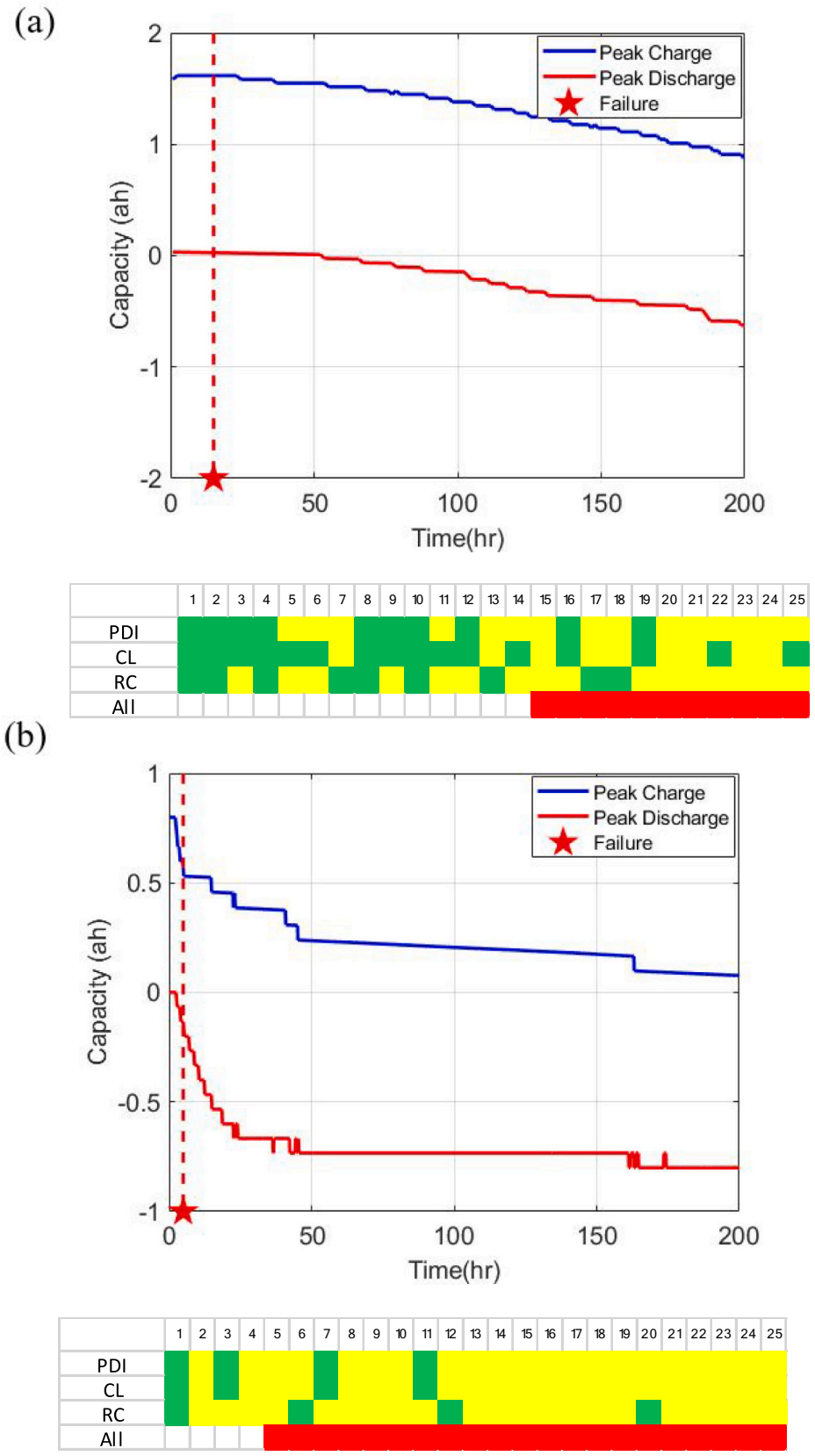

Fig. 8. Composite failure prediction of DDP for: a) 48D battery @ 1C, b) 54D battery @ 2C.

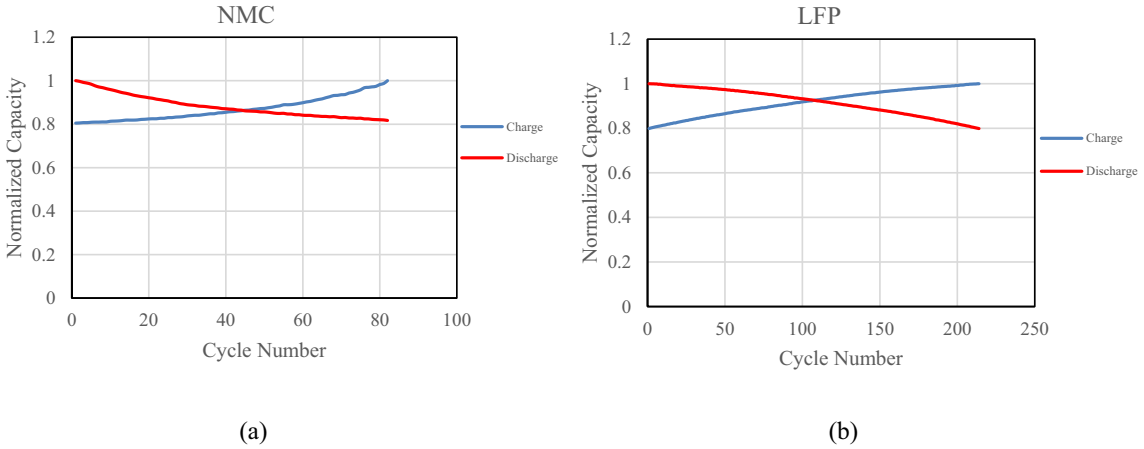

Fig. 9. Normalized charge discharge capacity for (a) NMC and (b) LFP batteries.

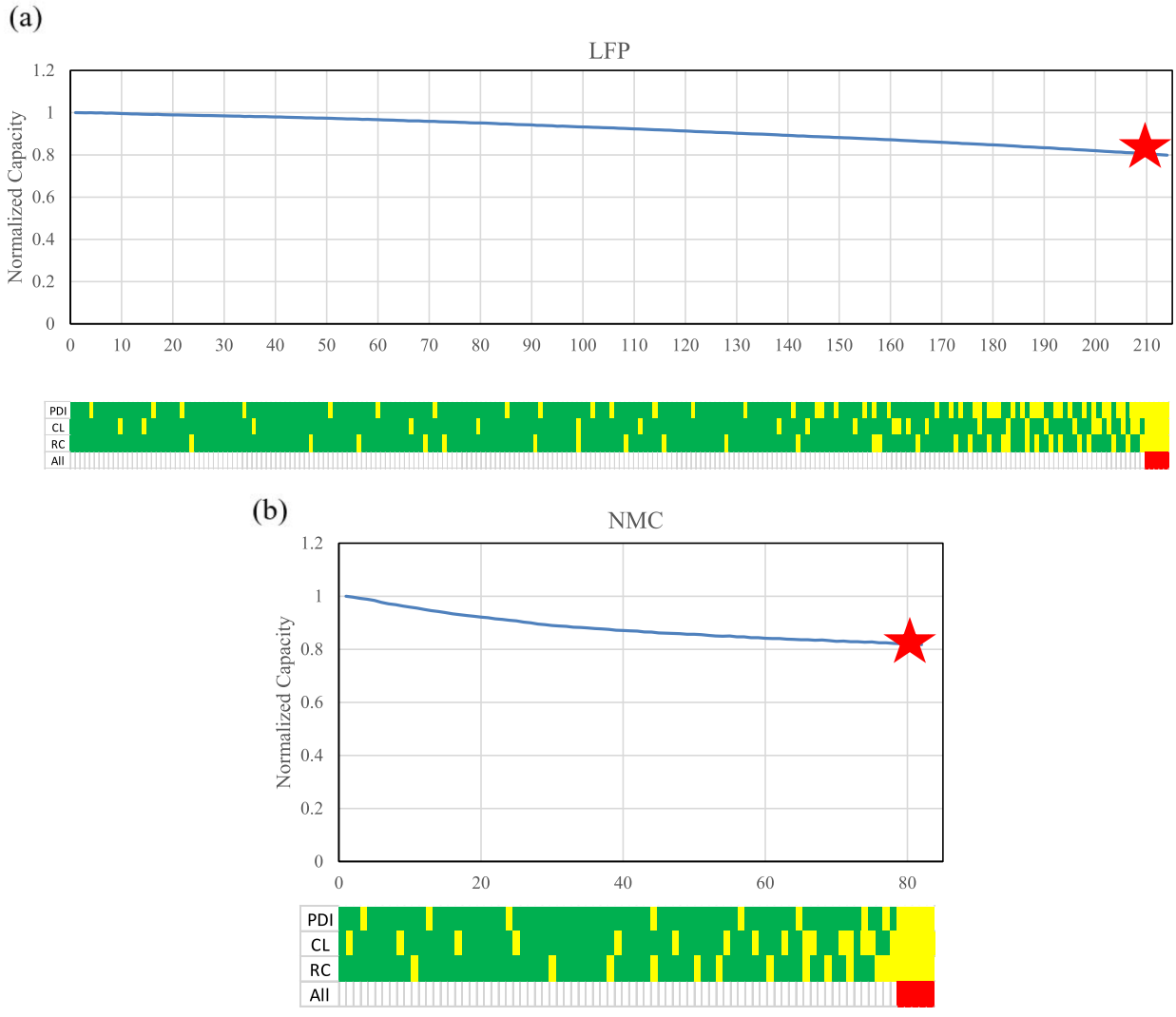

Fig. 10. Composite failure prediction of DDP for: a) LFP battery, b) NMC battery.

cycles (@ 0.5C charge and discharge). Data collection used a Neware BTS5V6A8CH battery testing system. Constant Current Constant Voltage (CCCV) charging and discharging protocol was adopted for all tests. The test included loading and unloading the cells to their cut-off voltage and subsequently charging them to their maximum safe voltage (100 % SOC). Then, the Vencon recharges the cells to 30 % SOC in order for safe storage. Furthermore, each step is performed based on the battery specifications and desired test (for instance, maximum C-rating).

In order to define the battery failure, we have considered the exceedance of capacity loss >80 % with respect to original capacity as the

failure point. Owing to the fact that the selected batteries were already ages and not much capacity was left in the devices, it was expected that the batteries will reach this threshold fairly soon. Furthermore, we carried out model validation by performing an additional analysis using the DDP for brand new batteries with the results shown in the next sections.

4. Results and discussion

After the batteries were analyzed, the results of the experimental tests were extracted. The extracted battery data are voltage, current, charge, and discharge capacity. Fig. 1 shows the variation of peak charge and discharge capacity for the battery cycling in 48 days (i.e., 48D) @ 1C and 54 days (i.e., 54D) @ 2C and voltage graphs of batteries for the first 1500 and 1000 min of cycling. According to the nominal capacity value of the batteries which was 2.1 Ah, after performing the experimental tests, it was witnessed that the capacity values started from 1.7 Ah for the 48D battery at 1C and 0.8 Ah for the 54D battery at 2C which indicate that the batteries are already crossed the end of life threshold. The results are shown in Fig. 1.

4.1. Path dependency index (PDI)

As described in the model development section, first the long-term and short-term ranks are computed using the constructed global matrix and Eqs. (1) & (2) at each instant of time. Using the two obtained values, the conservation principle is enforced at each point and the dimensionless length scales (dilatational and distortional) using the given Poisson's ratios are obtained, allowing for the calculation of local curvature. The obtained local curvature information is then used to compare the curvature values with the critical threshold (denoted by the reciprocal of the length scale). Based on the comparison results, each point at a specific root is assigned a PDI category based on Table 1 to evaluate the amount of instability that occurs at each point. A PDI >5 represents local instability in the system with the potential to transcend to global instability. Next, consistent with the assumption of piecewise second-order utility function around each observation, the zoom-out aggregation procedure is followed. This procedure is done to identify the critical chain length in the system defined as the magnitude of energy exchange pathway required for a local instability to transcend to global scales. Coupling occurrence of chain length greater than the critical value in addition to the exceedance of energy exchange rate through such a pathway, constitutes the global instability in the system. Such critical energy release rate is an inherent property that is normally calculated through offline testing. In this work, instead of such offline measurement, it is conjectured that almost all of the energy stored along such a pathway gets released when the local instabilities transition to global scales. Hence, during such transcendent, the energy exchange rate fluctuates rapidly and reaches zero. This rapid energy exchange rate is used in the scheme as the instant that energy drops >80 % at a time instant. Selection of such a rate is arbitrary in this method, alluding to the inherent noise floor in the procedures. The results of the PDI categorization are shown in Fig. 2 for the batteries. The figure demonstrates the percentage of points reaching a specific PDI for different time instants. Based on the results of the PDI calculation, the system enters the path dependency phase in its initial stages.

The figure illustrates the number of roots that have a PDI category larger than 5 only without the chain length information considered. The times when the roots are equal to and >50 % in number of points, is said to be path dependent. The system is said to be path-dependent if at least one point in the observation body is path-dependent. Fig. 3 shows the plots that highlight the moments when the batteries might have become path-dependent only. In other words, they show the number of roots with a PDI category >5 without the chain length information. Based on the results, the systems in both cases enter the path dependency at their early stage.

4.2. Chain length formation

Fig. 4 illustrates the number of roots that had PDI $\geq$ 5 and also crossed the critical chain length threshold (22 in the battery system). The value of critical chain length is calculated from the zoom-out plot which is shown in Fig. 6, as a sample plot for an arbitrary dimension. After calculating the curvature values (κ or kappa) as well as short-term and long-term critical values which are denoted by ($\frac{1}{LBar}$, $\frac{1}{LBarTilda}$ respectively) at every aggregation level, the kappa graph is extrapolated in its opposite region using the symmetry condition. Then, $\frac{1}{LBarTilda}$ line is extended backwards until it intersects with the mirror line (around y-axis) of kappa graph. Then, the logarithmic value of this intersection is identified and considered as the number of points related to the aggregated frame and critical chain length value. Such a value provides an estimate for long-term critical chain length. Critical chain length is calculated to determine how long a defect continues in each direction in order of their ranks. The critical chain length depends on the number of chosen observation points. The instants of time when the roots are equal and >50 % (8 out of 16) in number, the system is said to be near failure in all those times. Based on the results, for both 48D and 54D batteries, the systems cross the long-term localization index at an early stage and this phenomenon is more severe for 54D batteries.

4.3. Residual curvature

As discussed in previous sections, Fig. 3 illustrates when the system is only path-dependent, while Fig. 4 illustrates when local instability might transcend to global instability by forming an energy exchange pathway longer than the critical threshold value. The residual curvature results for the systems at different time indices are shown in Fig. 5. The residual curvature concept is used herein to provide a dimensionless aggregated measure of the magnitude of the energy exchange rate for the system. According to this concept, if the residual curvature surpasses a critical threshold value, the local instability can transcend to global instability in the system.

Here, another fact was used is that the stored energy in the system is depleted rapidly during such global transcendation. Thus, the rate of change, such rapid drop, is constantly monitored to detect any imminent failure of the system. At time instances in which this rapid drop exceeds >80 %, it is said that the system is progressing toward failure. After each time instant was analyzed, the results were obtained and shown in Fig. 5, which shows the percentage of a total number of roots (out of 64) in all four dimensions of the battery that had a drop of residual curvature larger than 80 %. The battery will dissipate a large amount of energy if the number of roots reaches a value larger than 20 % (12 out of 64 roots).

4.4. Critical localization index

The zoom out plots, as stated previously, are used to calculate the critical chain length in the system. Based on the results of the critical chain length calculation shown in Fig. 6 for 48D battery in an arbitrary dimension, the number for the critical chain length can be obtained and converted to a number corresponding to the number of observation points were considered for the lithium-ion batteries. The number derived from Fig. 6 represents the critical chain length for 9 points and later converted to match the number of points considered for the system. This number is considered for the chain length algorithm to determine how many points form a chain that is larger than the calculated value.

4.5. Composite failure prediction

The final failure prediction of the batteries takes all the above analysis into account in order to make a prognostication about the system as to when is the most probable time that it fails. The results are

shown for 48D and 54D batteries in Figs. 7 and 8. To prognosticate the failure, the system first needs to enter the path dependency phase. Then, if the chain formed at each time instant exceeds the critical chain length in both short-term and long-term phases, the dislocations have the potential to form a line defect which can cause failure in the system.

Furthermore, the system needs to have greater energy absorption or release than the critical energy exchange rate. Such activity is seen through large and rapid drops in residual curvature. A drop of larger than 80 % is used here as a trigger in the system. Once both of these criteria are met (GTI $>$ 0) after the system entered the path dependency mode (PDI $>$ 5), failure can be predicted for the system. In the battery prognostics, the systems were under constant monitoring when it entered the path dependency stage. Based on the results, for the 48D battery, the system is supposed to fail at time instant 15, while for the 54D battery, the system is expected to fail at time instant 5 which was expected as the batteries were already aged and did not contain much capacity. The prognostications were validated by comparing the results with the experimental testings. The failure of LIBs is defined as the moment when the full charging capacity reaches 80 % of the rated value which is a common threshold in most applications. As such, this threshold was chosen as the end of life (EOL) of LIBs. According to the results, both batteries fail in the initial stages of cycling which aligns with DDP results. Taking into account all of the failure criteria for the batteries, the results are compiled and shown in Fig. 8. In the figure, the critical instances for each criterion, i.e. PDI, chain length and residual curvature are shown with yellow color indicating exceeding the limit and green color noting not a critical region.

4.6. Further estimation of battery failure

In order to validate the DDP results and provide a further estimation of the battery failure, additional simulations were carried out on new batteries. For this purpose, two batteries with polymer electrolyte were chosen with the cathode made of lithium nickel cobalt manganese oxide (NCM) and lithium iron phosphate (LFP). The cut-off voltage range for NMC was between 3.0 and 4.2 V and for LFP was between 2.0 and 3.65 V. Nanocomposite polymer electrolytes (CNPEs) based on polyethylene oxide were used for the electrolyte with the tests being stopped when the charge capacity of the batteries were dropped to 80 % of the initial capacity which was 82 cycles for the NMC battery and 230 cycles for the LFP battery. The data that were used for the DDP were extracted from [44] with the normalized capacity graphs shown in Fig. 9. The features that were fed to the algorithm were charge discharge capacity and impedance information from the experimental tests.

The results of the simulations for the selected batteries are shown in Fig. 10 that are compiled in a single graph. As shown in the results, the DDP predicted the failure of the batteries accurately before the actual failure of the batteries. The yellow color in the prognostication chart depicts the instance that the corresponding criteria of the DDP are met and the red color indicates the onset of failure in which the operation of the batteries needs to be stopped.

5. Conclusions

One of the main obstacles in the further adaptation of the current electric vehicle market is the reliability and safety of battery packs. A universal solution for safe operation and accurate monitoring of batteries is the implementation of PHM frameworks. This study proposed and employed a novel data-driven method to analyze the health status of Li-ion batteries. The method is suitable for handling multi-scale and multi-physics problems that is based on data gathered in a continuous process. Unlike many PHM methodologies that rely on the system's available information or constitutive parameters obtained by offline testing, the proposed scheme obviates the need for a priori offline testing by pursuing a deterministic approach considering two consecutive time sequences at each step. The developed method was then used to monitor the performance of lithium-ion batteries by making a prognostication as to when is the most probable time that the batteries will fail. Experimental data from battery cycling were fed into the algorithm which were voltage, current and charge discharge capacity. DDP uses these information to detect excessive deviation from the critical threshold represented by system curvature. Based on the results obtained, it has been proven that DDP was able to predict the failure of the batteries prior to the actual failure. The results were validated by conducting a model verification scheme that confirmed the efficacy of the framework. The proposed method can substantially contribute the increase in the advancements of PHM techniques and ensure the safety and reliability of lithium ion batteries.

Declaration of competing interest

The authors declare that they have no known competing financial interests or personal relationships that could have appeared to influence the work reported in this paper.

Data availability

Data will be made available on request.

Acknowledgements

L.L. appreciates the support from the National Science Foundation under Award #1840732, KS NASA EPSCoR Program, Kansas Soybean Commission, KU ASCEND Award, KU RISe Award, KU Research GO awards, and KU General Research Funds. Any opinions, findings, and conclusions or recommendations expressed in this material are those of the author(s) and do not necessarily reflect the views of the funding agencies.

References

[1] EDTA, Electric Drive Transportation Association (EDTA), Washington Dc. 2021.
[2] BloombergNEF, Electric Vehicle Outlook, BloombergNEF (BNEF), 2021.
[3] IEA, Global EV Outlook 2020: Entering the Decade of Electric Drive?. International Energy Agency (IEA), Technology Report, 2020.
[4] L.G. Lu, A review on the key issues for lithium-ion battery management in electric vehicles, J. Power Sources 226 (2013) 272–288.
[5] K. Forrest, Estimating the technical feasibility of fuel cell and battery electric vehicles for the medium and heavy duty sectors in California, J. Appl. Energy (2020) 276.
[6] M.B. Pinson, M. B., Theory of SEI formation in rechargeable batteries: capacity fade, accelerated aging and lifetime prediction, J. Electrochem. Soc. 160 (2012) A243–A250.
[7] L. Liu, J. P, X. Lin, A.M. Sastry, W. Lu, A thermal-electrochemical model that gives spatial-dependent growth of solid electrolyte interphase in a Li-ion battery, J. Power Sources 268 (2014) 482–490.
[8] P. Guan, L. L, X. Lin, Simulation and experiment on solid electrolyte interphase (SEI) morphology evolution and lithium-ion diffusion, J. Electrochem. Soc. 162 (2015) A1798–A1808.
[9] U.R. Koleti, T.Q. D, J. Marco, A new on-line method for lithium plating detection in lithium-ion batteries, J. Power Sources 451 (2020), 227798.
[10] B.L.D. Rinkel, D.S. H, I. Temprano, C.P. Grey, Electrolyte oxidation pathways in lithium-ion batteries, J. Am. Chem. Soc. 142 (2020) 15058–15074.
[11] C.R. Birkl, R. M, E. McTurk, P.G. Bruce, D.A. Howey, Degradation diagnostics for lithium ion cells, J. Power Sources 341 (2017) 373–386.
[12] M. Celina, Lithium-ion Batteries Hazard and Use Assessment, Springer, US, 2011.
[13] L. Liu, M. Z, Modeling of SEI layer growth and electrochemical impedance spectroscopy response using a thermal electrochemical model of Li-ion batteries, ECS Trans. 61 (2014) 43–61.
[14] W. He, W. N, M. Osterman, M. Pecht, Prognostics of lithium-ion batteriesbased on Dempster–Shafer theory and the Bayesian Monte Carlo method, J. Power Sources 196 (2011) 10314–10321.
[15] A. Barré, D. B, S. Grolleau, M. Gérard, F. Suard, D. Riu, A review on lithiumion battery ageing mechanisms and estimations for automotive applications, J. Power Sources 241 (2013) 680–689.
[16] Y. Li, V. M, S.S. Choi, T.W. Farrell, N.T. Tran, J. Teague, Development of a degradation-conscious physics-based lithium-ion battery model for use in power system planning studies, Appl. Energy 248 (2019) 512–525.
[17] A. Maheshwari, Optimizing the operation of energy storage using a non-linear lithium-ion battery degradation model, Appl. Energy 261 (2020), 114360.

[18] X. Lin, J. P, L. Liu, Y. Lee, A.M. Sastry, W. Lu, A comprehensive capacity fade model and analysis for Li-ion batteries, J. Electrochem. Soc. 160 (2013) A1701–A1710.
[19] S. Saxena, Y. X, M.G. Pecht, PHM of Li-ion Batteries Prognostics and Health Management of Electronics, Wiley, 2018, pp. 349–375.
[20] S. Cheng, M.H. A, M.G. Pecht, Sensor systems for prognostics and health management, Sensors 10 (2010) 5774–5797.
[21] J. Liu, D. D, K.A. Marko, J. Ni, Mech. Syst. Signal Process. 23 (2009) 2488–2499.
[22] J. Guo, L. Z, M. Pecht, A Bayesian approach for Li-ion battery capacity fade modeling and cycles to failure prognostics, J. Power Sources 281 (2015) 173–184.
[23] G.J. Vachtsevanos, F. L, A. Hess, B. Wu, Intelligent Fault Diagnosis and Prognosis for Engineering Systems, Wiley Online Library, 2006.
[24] M.A. Toufik Aggab, Pascal Vrignat, Frédéric Kratz, Unifying model-based prognosis with learning-based time-series prediction methods: application to Li-ion battery, IEEE Syst. J. 15 (4) (2021) 5245–5254.
[25] Y.F. Weihan Li, Florian Ringbeck, Dominik Jöst, Dirk Uwe Sauer, Unlocking electrochemical model-based online power prediction for lithium-ion batteries via Gaussian process regression, Appl. Energy 306 (2022).
[26] J.T. Rui Xiong, Hao Mu, Chun Wang, A systematic model-based degradation behavior recognition and health monitoring method for lithium-ion batteries, Appl. Energy 207 (2017).
[27] R.X. Zeyu Chen, Jinpeng Tian, Xiong Shang, Jiahuan Lu, Model-based fault diagnosis approach on external short circuit of lithium-ion battery used in electric vehicles, Appl. Energy 184 (2016) 365–374.
[28] B. Saha, K. G, S. Poll, J. Christophersen, Prognostics methods for battery health monitoring using a Bayesian framework, IEEE Trans. Instrum. Meas. 58 (2008) 291–296.
[29] P. M, Prognostics and Health Management of Electronics, Wiley Interscience, New York, NY, 2008.
[30] J. Wu, Z. C, Z. Chen, An online method for lithium-ion battery remaining useful life estimation using importance sampling and neural networks, Appl. Energy 173 (2016) 134–140.
[31] M.E. T, The Relevance Vector Machine: Advances in Neural Information Processing Systems, 2000, pp. 652–658.
[32] Rasmussen Carl Edward, W.C. K, Gaussian Processes for Machine Learning, MIT Press, 2006.
[33] F. Cadini, C. S., F. Cancelliere, M. Giglio, State-of-life prognosis and diagnosis of lithium-ion batteries by data-driven particle filters, Appl. Energy 235 (2019) 661–672.
[34] F.Y. Guangzhong Dong, Zhongbao Wei, Jingwen Wei, Kwok-Leung Tsui, State-of-life prognosis and diagnosis of lithium-ion batteries by data-driven particle filters, Appl. Energy 235 (2020) 661–672.
[35] Y. Zhao, L. P, Z. Wang, L. Zhang, J. Hong, Fault and defect diagnosis of battery for electric vehicles based on big data analysis methods, Appl. Energy 207 (2017) 351–362.
[36] M.S. Hossain Lipu, M.A. H, A. Hussain, A. Ayob, M.H.M. Saad, T.F. Karim, N. T. Dickson, How data-driven state of charge estimation of lithium-ion batteries: algorithms, implementation factors, limitations and future trends, J. Clean. Prod. 277 (2020), 124110.
[37] A. Chandra, K. O, Data driven prognosis: a multi-physics approach verified via balloon burst experiment, Proc. R. Soc. A 471 (2176) (2015).
[38] A. Chandra, K. O, K.-C. Wu, M. Hall, J. Gillette, Prognosis of anterior cruciate ligament reconstruction: a data-driven approach, Proc. R. Soc. A 471 (2015), 20140526.
[39] A. Chandra, R. S, On removing Condorcet effects from pairwise election tallies, Soc. Choice Welf. 40 (2013) 1143–1158.
[40] A. Chandra, K. P, M. Dorothy, Implications of Arrow's theorem in modeling of multiscale phenomena: an engineering approach, in: NSF-DMMI Grantee Conference, Knoxville, TN, 2008.
[41] S. DG, Explaining all three alternative voting outcomes, J. Econ. Theory 87 (1999) 313–355.
[42] S. DG, Chaotic Elections! A Mathematician Looks at Voting, , American Mathematical Society, Providence, RI, 2001.
[43] M.H. Sadd, Elasticity Theory, Applications, and Numerics, Elsevier, 2014.
[44] D. Cheng, W. Sha, L. Wang, S. Tang, A. Ma, Y. Chen, H. Wang, Solid-state lithium battery cycle life prediction using machine learning, Appl. Sci. 11 (4671) (2021).